Title
Fixed Beamline Optimization for Intensity Modulated Carbon-Ion Therapy

Journal
IEEE Transactions on Radiation and Plasma Medical Sciences, 6(3)

ISSN
2469-7311

Authors
Ramesh, Pavitra
Liu, Hengjie
Gu, Wenbo
et al.

Publication Date
2022-03-01

DOI
10.1109/trpms.2021.3092296

Peer reviewed

HHS Public Access

Author manuscript

IEEE Trans Radiat Plasma Med Sci. Author manuscript; available in PMC 2023 March 01.

Published in final edited form as:

IEEE Trans Radiat Plasma Med Sci. 2022 March ; 6(3): 288–293. doi:10.1109/trpms.2021.3092296.

Fixed Beamline Optimization for Intensity Modulated Carbon-Ion Therapy

Pavitra Ramesh,
Physics and Biology in Medicine interdepartmental program, University of California Los Angeles, Los Angeles, CA 90025 USA

Hengjie Liu,
Physics and Biology in Medicine interdepartmental program, University of California Los Angeles, Los Angeles, CA 90025 USA

Wenbo Gu,
Department of Radiation Oncology, University of Pennsylvania, Philadelphia, PA 19104 USA

Ke Sheng
Physics and Biology in Medicine interdepartmental program, University of California Los Angeles, Los Angeles, CA 90025 USA

Abstract

A major obstacle for the adoption of heavy ion therapy is the cost and technical difficulties to construct and maintain a rotational gantry. Many heavy ion treatment facilities instead choose to construct fixed beamlines as a compromise, which we propose to mitigate with optimized treatment couch angle. We formulate the integrated beam orientation and scanning spot optimization problem as a quadratic cost function with a group sparsity regularization term. The optimization problem is efficiently solved using fast iterative shrinkage-thresholding algorithm (FISTA). To test the method, we created the fixed beamline plans with couch rotation (FBCR) and without couch rotation (FB) for intensity modulated carbon-ion therapy (IMCT) and compared with the ideal scenario where both the couch and gantry have 360 degrees of freedom (GCR). FB, FBCR, and GCR IMCT plans were compared for ten pancreas cases. The FBCR plans show comparable PTV coverage and OAR doses for each pancreas case. In conclusion, the dosimetric limitation of fixed beams in heavy ion radiotherapy may be largely mitigated with integrated beam orientation optimization of the couch rotation.

Index Terms—

beam orientation; carbon ion; gantry; heavy ion; optimization

correspondence: ksheng@mednet.ucla.edu.

I. Introduction

Carbon-ion therapy has been increasingly garnering attention worldwide due to its superior physical dose distributions and high relative biological effectiveness (RBE). Compared to photon and electron beams, proton and carbon ion beams are more conformal to tumors because they deliver most of their dose in well-defined Bragg peaks, therefore possessing the ability to localize their deposition of energy within deep-seated tumors [1–3]. About 85% of cancer patients receiving particle therapy are irradiated with protons, which have physical advantages compared to photons, but a similar biological response [2]. Carbon ions, however, have a steeper lateral fall-off and smaller penumbra than proton beams, which offers a better potential for targeting tumors that are close to critical structures [4]. The radiobiological effectiveness (RBE) of carbon ion rise substantially along the beam direction and reaches its maximum near the Bragg peak, further increasing the therapeutic ratio compared with the proton beams whose RBE varies more moderately. Heavy ions are particularly attractive for treating radioresistant tumors, and carbon ion therapy may promote immune response and reduce angiogenesis and metastatic potential [2,5,6]. Through clinical studies, carbon ion beams have been able to reduce treatment time and toxicities [1], making it the desirable treatment modality in terms of efficiency and dosimetry.

However, the access to carbon-ion therapy is greatly hampered by its prohibitive cost, engineering challenges and space requirement, despite its unique potential to treat hypoxic and radioresistant tumors. Among the facilities of carbon-ion therapy, the fully rotational gantry is especially expensive, complex and space consuming due to the large magnets needed to bend the high energy carbon ion beams with high magnetic rigidity. Compared with protons, to reach the same depth, the magnetic rigidity of carbon ions is 2.5 times greater, demanding corresponding more powerful and larger magnets for beam bending and steering. As a result, the carbon gantry in the Heidelberg Ion Therapy (HIT) facility occupies 22 m long and 14 m high space and weights a total of 600 tons [7]. Equipment and building costs, in particular, are extremely high [8,9]. The gantry weight can be reduced using superconducting magnets. For example, the superconducting carbon ion gantry at the National Institute of Radiological Sciences (NIRS) in Japan weighs 300 tons [10,11] due to the use of superconducting magnets, which are costly to build and operate, and still significantly heavier than a proton gantry. Further engineering challenges include maintaining the targeting accuracy with gantry rotation. There are limited existing solutions available for equipment and treatment planning software troubleshooting by suppliers.

The current debate at many cancer treatment centers in relation to carbon ion therapy is whether the installation of a gantry is feasible. Compared with the gantry systems, fixed-beam port systems significantly simplify the system design for carbon ion therapy and are more widely employed in most carbon ion centers for treatment delivery at the moment. However, the fixed beam line design has been considered a significant compromise in flexibility and achievable dosimetry. Once built, the directions of fixed beamlines cannot be modified. The unclear magnitude of performance degradation and lack of systematic approach to mitigate the compromise could dampen the enthusiasm for carbon ion system adoption.

Carbon ion centers are employing the use of a single horizontal beam (90°), some with an additional vertical beam (0°) [12,13]. Kosaki et al. compared intensity modulated proton therapy (IMPT) plans for the treatment of skull base meningioma and found that excellent dose distributions can still be achieved with one fixed beam [13]. To determine if there is a superior fixed beamline configuration for a typical two beamline configuration, Koom et al. performed a dosimetric comparison among seven fixed beam angles (340°, 315°, 0°, 20°, 45°, 90°, 180°) in the prone position with carbon ion pencil beam scanning for pancreatic cancer[14]. CTV or GTV coverage among the 7 beams did not widely differ. Dose to the descending duodenum were high with 45° and 90°, but lower for the ascending duodenum compared to the 180° beam. 20° and 315° seemed to be better for the stomach. Some facilities add a rotating couch to up to 45° as a non-gantry solution [15]. The addition of a 45° beam to the 90° beam in our study would allow for variability in the couch rotation, while keeping the value of a vertical beam.

The current study attempts to answer a different question using a carbon ion system with 360 degrees as the reference, which is the potential to mitigate or eliminate the dosimetric disparity with optimized combination of the fixed beam and couch angles. Although the combination has a relatively limited solution space compared with a full gantry system, it still includes more than a hundred available beam directions for optimization.

To achieve the optimization goal, we exploited the couch rotation freedom with an automated IMCT beam orientation optimization (BOO) method.

II. Methods

A. Beam Geometry

The gantry-based plan starts with 1162 non-coplanar beams uniformly distributed across the 4π steradians with 6° separation between adjacent beams combining the gantry and couch rotational degrees-of-freedom. Beam screening is performed to remove beams with infeasible energies or impractical entries into the body, such as those going through the head or feet, leaving 420 beams in the candidate set. For the fixed-beamline plans, we select by hand a total of 90 beams, 30 from the 90° gantry angle, and 60 from the 45° angle. From this, we compared plans with no couch kick against plans with couch angles ranging from 0° to 360° with 6° interval. Note that the possible gantry angles for fixed beam plans, with couch rotation (FBCR) and without (FB), are not an exact subset of the angles for the gantry couch rotation (GCR) plan as shown in Fig. 1 due to discretization and finite spacing between beams.

For each candidate beam, carbon ion pencil beam dose calculation for the scanning spots covering the PTV and a 5mm margin was performed using matRad [16,17], a MATLAB-based 3D treatment planning toolkit. The physical dose calculation matrix A, which includes all candidate beams, was generated in this calculation, with an isotropic resolution of 2.5 mm, along with α and β matrices for carbon ion, characterizing the radiosensitivity of the tissue based on the linear quadratic model for survival fraction. Our optimization was formulated to select one or two beams from the candidate beam pool.

B. Beam Orientation Optimization

Beam orientation optimization (BOO) was performed for GCR, FB, and FBCR plans under the same optimization framework [18,19]. Assuming $\mathscr{B}$ is the set containing all the feasible candidate beams, the BOO problem is described as follows:

$$\begin{aligned} &\underset{\boldsymbol{x}}{\text{minimize}} \sum_{k \in \mathscr{T}} \alpha_k \|A_k \boldsymbol{x} - p_k\|_2^2 + \sum_{k \in \mathscr{O}} \alpha_k \|(A_k \boldsymbol{x} - q_k)_+\|_2^2 + \sum_{b \in \mathscr{B}} \lambda_b \|\boldsymbol{x}_b\|_2^{1/2} \\ &\text{subject to } \boldsymbol{x} \geq 0 \end{aligned} \tag{1}$$

where $\boldsymbol{x}_b$ is a vector that represents the scanning spot intensities for each candidate beam b, and the optimization variable $\boldsymbol{x}$ is the concatenation of all the vectors $x_b (b \in \mathscr{B})$. The dose calculation matrix A includes all the candidate beams along the column direction, with the product of A and x being dose to each voxel. $\mathscr{T}$ is the set including the target volumes and $\mathscr{O}$ is the set including the organs at risk (OAR). Once a fluence map was obtained, the plans were weighted with RBE values calculated for each structure k from the α and β matrices, using the following model [20]:

$$\begin{aligned} -\ln(S) &= (\beta_C D_C + \alpha_C) D_C \\ D_{bio} &= \sqrt{-\frac{\ln(S)}{\beta_x} + \left(\frac{\alpha_x}{2\beta_x}\right)^2} - \frac{\alpha_x}{2\beta_x} \end{aligned} \tag{2}$$

where D_C is fractional carbon physical dose, α_x and β_x are biological parameters of the LQ model for photon as a reference radiation and α_C and β_C are the parameters for carbon ion. For pancreatic cancer, α_x is 0.015 Gy^{-1} and β_x is 0.0016 Gy^{-2} [21]. For the gastrointestinal tract and spinal cord, respectively, α_x values are [0.087, 0.0445] Gy^{-1} and β_x values are [0.013, 0.0135] Gy^{-2} [22].

The first two terms in (1) represent dose fidelity. The first term penalizes any dose deviation from prescription dose p_k for target k to ensure a homogeneous physical dose distribution in the target. The second term encourages any dose in the OAR k to not exceed the maximum allowable dose for that OAR, q_k. The last term $\sum_{b \in \mathscr{B}} \lambda_b \|\boldsymbol{x}_b\|_2^{1/2}$ is an L2,1/2-norm group sparsity term. We set the value for the weighting hyperparameter, λ_b, for each beam such that most $\boldsymbol{x}_b$ are penalized to be identically zero. Subsequently, most of the candidate beams were turned off, leaving only one or two beams active. Weighting for group sparsity is turned off when further fluence map optimization is performed once beams are selected.

Carbon ion beam angle selection and fluence map optimization were performed simultaneously to generate a plan with acceptable dosimetry. FISTA, an accelerated proximal gradient method known as the Fast Iterative Shrinkage-Thresholding Algorithm [23] was used to solve this non-differentiable problem.

C. Patient Evaluations

We compared the GCR, FB, and the proposed FBCR method for ten pancreatic cases initially planned for photon radiotherapy. The original prescription dose was 33 Gy with selective simultaneous integrated boost (SIB) dose to 40 and 50 Gy. Since the prescription dose is not used for carbon ion and the purpose of the study was not to compare with the

photon doses, all plans were prescribed to a total dose of 52.8 GyRBE in 12 fractions [24]. The goal for the PTV dose was to cover 90% of the PTV with 95% of the prescription dose. The target volumes and average spot count per beam for each patient are shown in Table I. For all plans, biological dose (GyRBE) was evaluated. Similar structure weighting was used across plans to ensure unbiased comparison. For each pancreatic case, PTV homogeneity, D95%, and mean dose to the PTV, as well as the maximum dose received by 2cc of the stomach, bowel and duodenum was evaluated. The PTV homogeneity index (HI) is defined as D95%/D5%. The mean and maximum doses for OARs were also evaluated. Maximum dose is defined as the dose to 2% of the structure volume, D2%, following the recommendation by ICRU 83 [25]. The upper clinical goal for all gastrointestinal tract (GI) organs was 46 GyRBE. Maximum dose to the spinal cord limit was 30 GyRBE [24].

III. Results

A. Runtime and Optimization of Beams

The dose calculation and optimization processes were performed on an 8-core CPU workstation. To calculate the dose and biological parameter matrices for all candidate beams for each approach, the MATLAB Parallel Computing Toolbox was used to accelerate the computation. The times spent on dose calculation and BOO are listed in Table II along with the gantry and couch angles chosen during beam selection. Since the number of candidate beams for the fixed beam approaches were significantly reduced, dose calculation time was cut down by a factor of about 5. The FBCR plans have the potential to reduce beam orientation and fluence map optimization times with the pancreatic cases. For difficult FBCR plans, optimization may require a larger regularization parameter for the group sparsity term and possibly more time than a GCR plan to force convergence from 90 beams to only one or two beams while maintaining dosimetric integrity. While the addition of more beams will reduce the effort, we require that all plans select 1–2 beams for ease of delivery and comparison. In general, total effort for GCR plans takes on average 28 more minutes than FBCR plans. FBCR only takes about 30 more seconds compared to FB to select beams.

B. Dose Comparison

The optimized FBCR delivery is compared with the GCR and FB deliveries. An isodose comparison in the transverse, coronal, and sagittal planes can be viewed in Fig. 2. Overall, PTV coverage and OAR sparing varies between plans. A dose-volume histogram representing patient F is shown in Fig. 3 to compare biological dose structure-by-structure.

Fig. 4 shows PTV homogeneity (HI), mean, and maximum biological dose to the PTV for all plans. PTV coverage was significantly better with GCR and FBCR compared to FB. Paired t-test was performed between GCR and FBCR, showing p-values of [0.19, 0.29, 0.12] for HI, mean, and maximum biological dose, respectively. The result indicates that the PTV metric differences are statistically insignificant between GCR and FBCR. On the other hand, the comparison between FBCR and FB had p-values of [0.02, 0.02, 0.35], indicating significantly higher HI and mean PTV doses with FBCR. Table III lists OAR statistics for the gastrointestinal tract and spinal cord, which are lowest, in general, with the GCR plan. In all plans in which GCR met the clinical standard of less than 46 GyRBE to the GI

tract, FBCR was able to do so as well. Compared with FB plans, FBCR reduced bowel, duodenum, and stomach doses by [27%, 12%, 23%] and GCR reduces the doses by [35%, 16%, 43%]. P-values for bowel, duodenum, and stomach were [0.02, 0.16, 0.05] between GCR and FBCR and [0.07, 0.33, 0.12] between FBCR and FB, showing mostly minor improvements in dose from FB to FBCR and from FBCR to GCR. For liver and kidneys, mean dose difference between all plans is less than 1 GyRBE. All plans met the clinical limit of 30 GyRBE for the maximum dose to the spinal cord. We have shown a significant improvement of FBCR over FB plans. The OAR sparing gains by FBCR were [77%, 75%, 53%] of that by GCR for the bowel, duodenum, and stomach, respectively.

IV. Discussion

We performed the study to investigate the dosimetric implications of fixed beamlines vs. gantry IMCT plans for the pancreatic cancer treatment. We adopted our previously published beam orientation optimization method to solve a new problem, which is the carbon ion beam orientation optimization with fixed beamlines. The new problem can be considered a subproblem of the full BOO problem with limited degrees of freedom. The additional degree of freedom reduced the gap in solution spaces between the gantry and fixed beamline plans. The large solution space precludes effective manual beam orientation selection. We solved the integrated BOO and scanning spot optimization problems using group sparsity regularization for both the GCR and FBCR plans. We showed that the dosimetric difference between gantry and fixed beamline IMCT may be substantially narrowed if the couch rotation can be fully exploited by solving the optimization problem.

In this study, we specifically choose 45° and 90° polar beamlines for our fixed-beam approach. While it is possible that changing the combination of beamline angles may result in tumor coverage and normal tissue sparing, this effect can dependent on patient characteristics and local anatomy configurations. In theory, 90° beam allow sampling of the most widespread of the spherical space in combination with the couch rotation. Smaller angles would reduce the radiological path lengths for oblique beams, but too small a polar angle would result in a collapsed cone and degenerated solution space. Therefore, the 45° −90° orientations seem to be a well-balanced and generalizable combination. A rigorous conclusion for the fixed-beamline orientation selection problem needs to be drawn based on a statistical analysis of the dosimetry for many more patient types and cases.

Besides limited patient cases, another limitation is that geometrically undesired beams and beams of infeasible energies were only partially excluded from the 1162-beam candidate set. These beams with long radiological pathlength are eliminated in BOO due to undesired geometry. Simulations that model three-dimensional collisions of large gantries with the patient and couch for different treatment zones have been performed for proton [26], but to our knowledge, no studies of this kind have yet been published for carbon ion gantries. Once carbon beam log data is available, more accurate beam screening should be performed for carbon gantries to assess the impact on beam selection and resulting dosimetry.

Solutions to the problem of having limited beam angles with fixed beamlines for carbon ion include rotating the couch along the long axis [27]. Couch rotation is commonly

used in clinical practice. With robotic couch, sub-millimeter movement accuracy has been demonstrated [28]. However, the couch motion may increase the probability of patient shift, which can be managed by immobilization and surface, X-ray, and tomographic imaging monitoring.

Due to the prohibitively long time required to calculate dose for 1162 candidate beams using Monte Carlo, the current study uses an analytical method, which is acceptable for dose comparison [19,29], but may have inaccuracies for further studies with biological objective functions due to its inability to account for fragmentation or secondary particles [30–32]. Either fast CPU- or GPU-based Monte Carlo for carbon-ion radiation therapy may be better suited for that goal [33,34]. Physical dose conformality is our current optimization objective with an estimate of variable RBE applied. This is likely an oversimplification for the carbon ion beams. Because of the drastic changes in RBE along the beam path, different beams may be selected if more accurate RBE is modeled within the BOO problem. For instance, RBE-weighted dose using the local effect model (LEMIV), repair-misrepair-fixation (RMF) model, or microdosimetric kinetic model (MKM) [35,36], can be used to explore the effectiveness of a biological dose optimization framework with the fixed beamline approach.

V. Conclusions

We show that the dosimetry compromise due to the fixed beamlines vs. a full gantry for carbon-ion therapy can be largely mitigated for pancreatic cases with the beam orientation optimization exploiting the couch rotation freedom. With further investigation on other disease sites, this work indicates the potential to significantly simplify gantry design for carbon-ion therapy, thus overcoming a major hurdle in availing this technology.

Acknowledgments

The study is supported in part by NIH R01CA230278

References

[1]. Tsujii H, Kamada T. A review of update clinical results of carbon ion radiotherapy. Jpn J Clin Oncol. 2012;42(8):670–685. doi:10.1093/jjco/hys104 [PubMed: 22798685]

[2]. Tinganelli W, Durante M. Carbon Ion Radiobiology. Cancers. 2020;12(10):3022. doi:10.3390/cancers12103022

[3]. Ohno T. Particle radiotherapy with carbon ion beams. EPMA J. 2013;4(1):9. doi:10.1186/1878-5085-4-9 [PubMed: 23497542]

[4]. Qin N, Shen C, Tsai M-Y, et al. Full Monte Carlo–Based Biologic Treatment Plan Optimization System for Intensity Modulated Carbon Ion Therapy on Graphics Processing Unit. Int J Radiat Oncol. 2018;100(1):235–243. doi:10.1016/j.ijrobp.2017.09.002

[5]. Ogata T, Teshima T, Kagawa K, et al. Particle Irradiation Suppresses Metastatic Potential of Cancer Cells. Cancer Res. Published online 2005:9.

[6]. Takahashi Y, Teshima T, Kawaguchi N, et al. Heavy Ion Irradiation Inhibits in Vitro Angiogenesis Even at Sublethal Dose. :6.

[7]. Th Haberer, Debus J, Eickhoff H, Jäkel O, Schulz-Ertner D, Weber U. The Heidelberg Ion Therapy Center. Radiother Oncol. 2004 Dec;73 Suppl 2:S186–90. doi: 10.1016/s0167-8140(04)80046-x. [PubMed: 15971340]

[8]. Durante M, Flanz J. Charged particle beams to cure cancer: Strengths and challenges. Semin Oncol. 2019;46(3):219–225. doi:10.1053/j.seminoncol.2019.07.007 [PubMed: 31451308]

[9]. Kamada T. Overview of the Heavy-Ion Medical Accelerator in Chiba (HIMAC) Practices. In: Tsujii H, Kamada T, Shirai T, Noda K, Tsuji H, Karasawa K, eds. Carbon-Ion Radiotherapy. Springer Japan; 2014:17–22. doi:10.1007/978-4-431-54457-9_3

[10]. Kirkby KJ, Kirkby NF, Burnet NG, et al. Heavy charged particle beam therapy and related new radiotherapy technologies: The clinical potential, physics and technical developments required to deliver benefit for patients with cancer. Br J Radiol. Published online October 6, 2020:20200247. doi:10.1259/bjr.20200247

[11]. Bhattacharyya T, Koto M, Ikawa H, et al. First prospective feasibility study of carbon-ion radiotherapy using compact superconducting rotating gantry. Br J Radiol. 2019;92(1103):20190370. doi:10.1259/bjr.20190370 [PubMed: 31317764]

[12]. Sheng Y, Sun J, Wang W, et al. Performance of a 6D treatment chair for patient positioning in an upright posture for fixed ion beam lines. Front Oncol. 2020;10. doi:10.3389/fonc.2020.00122

[13]. Kosaki K, Ecker S, Habermehl D, et al. Comparison of intensity modulated radiotherapy (IMRT) with intensity modulated particle therapy (IMPT) using fixed beams or an ion gantry for the treatment of patients with skull base meningiomas. Radiat Oncol. 2012;7(1):44. doi:10.1186/1748-717X-7-44 [PubMed: 22439607]

[14]. Koom WS, Mori S, Furuich W, Yamada S. Beam direction arrangement using a superconducting rotating gantry in carbon ion treatment for pancreatic cancer. Br J Radiol. Published online April 3, 2019:20190101. doi:10.1259/bjr.20190101

[15]. Zhang X, Hsi WC, Yang F. Development of an isocentric rotating chair positioner to treat patients of head and neck cancer at upright seated position with multiple nonplanar fields in a fixed carbon-ion beamline. Med Phys. 2020;47(6):2450–2460. doi:10.1002/mp.14115 [PubMed: 32141079]

[16]. Cisternas E, Mairani A, Ziegenhein P, Jäkel O, Bangert M. matRad - a multi-modality open source 3D treatment planning toolkit. In: Jaffray DA, ed. World Congress on Medical Physics and Biomedical Engineering, June 7–12, 2015, Toronto, Canada. IFMBE Proceedings. Springer International Publishing; 2015:1608–1611. doi:10.1007/978-3-319-19387-8_391

[17]. Wieser H-P, Cisternas E, Wahl N, et al. Development of the open-source dose calculation and optimization toolkit matRad. Med Phys. 2017;44(6):2556–2568. doi:10.1002/mp.12251 [PubMed: 28370020]

[18]. Gu W, O'Connor D, Nguyen D, et al. Integrated beam orientation and scanning-spot optimization in intensity-modulated proton therapy for brain and unilateral head and neck tumors. Med Phys. 2018;45(4):1338–1350. doi:10.1002/mp.12788 [PubMed: 29394454]

[19]. O'Connor D, Yu V, Nguyen D, Ruan D and Sheng K, Fraction-variant beam orientation optimization for non-coplanar IMRT, Phys Med Biol. 2018 Feb 15;63(4):045015. doi:10.1088/1361-6560/aaa94f [PubMed: 29351088]

[20]. Kramer M, Scholz M. Rapid calculation of biological effects in ion radiotherapy. Phys Med Biol. 2006;51(8):1959–1970. doi:10.1088/0031-9155/51/8/001 [PubMed: 16585839]

[21]. Prior PW, Chen X, Hall WA, et al. Estimation of the alpha-beta ratio for chemoradiation of locally advanced pancreatic cancer. Int J Radiat Oncol Biol Phys. 2018;102(3):S97. doi:10.1016/j.ijrobp.2018.06.250

[22]. Kehwar TS. Analytical approach to estimate normal tissue complication probability using best fit of normal tissue tolerance doses into the NTCP equation of the linear quadratic model. J Can Res Ther. 2005;1(3):168.doi:10.4103/0973-1482.19597.

[23]. Beck A, Teboulle M. A Fast Iterative Shrinkage-Thresholding Algorithm for Linear Inverse Problems. SIAM J Imaging Sci. 2009;2(1):183–202. doi:10.1137/080716542

[24]. Kawashiro S, Yamada S, Okamoto M, et al. Multi-institutional study of carbon-ion radiotherapy for locally advanced pancreatic cancer: Japan carbon-ion radiation oncology study group (J-CROS) study 1403 pancreas. Int J Radiat Oncol. 2018;101(5):1212–1221. doi:10.1016/j.ijrobp.2018.04.057

[25]. Hodapp N. [The ICRU Report 83: prescribing, recording and reporting photon-beam intensity-modulated radiation therapy (IMRT)]. Strahlenther Onkol. 2012 Jan;188(1):97–9. German. doi:10.1007/s00066-011-0015-x. [PubMed: 22234506]

[26]. Jung H, Kum O, Han Y, Park HC, Kim JS, Choi DH. A virtual simulator designed for collision prevention in proton therapy: A virtual simulator for proton therapy. Med Phys. 2015;42(10):6021–6027. doi:10.1118/1.4931411 [PubMed: 26429277]

[27]. Kumagai M, Mori S, Yamamoto N. Impact of treatment planning with deformable image registration on dose distribution for carbon-ion beam lung treatment using a fixed irradiation port and rotating couch. Br J Radiol. 2015;88(1050):20140734. doi:10.1259/bjr.20140734 [PubMed: 25811094]

[28]. Chan MF, Lim SB, Li X, Tang X, Zhang P, Shi C. Commissioning and Evaluation of a Third-Party 6 Degrees-of-Freedom Couch Used in Radiotherapy. Technol Cancer Res Treat. 2019;18:1533033819870778. doi:10.1177/1533033819870778 [PubMed: 31434547]

[29]. Gu W, Neph R, Ruan D, Zou W, Dong L, Sheng K. Robust beam orientation optimization for intensity-modulated proton therapy. Med Phys. 2019;46(8):3356–3370. doi:10.1002/mp.13641 [PubMed: 31169917]

[30]. Wilkens JJ, Oelfke U. Analytical linear energy transfer calculations for proton therapy. Med Phys. 2003;30(5):806–815. doi:10.1118/1.1567852 [PubMed: 12772988]

[31]. Kamp F, Cabal G, Mairani A, Parodi K, Wilkens JJ, Carlson DJ. Fast Biological Modeling for Voxel-based Heavy Ion Treatment Planning Using the Mechanistic Repair-Misrepair-Fixation Model and Nuclear Fragment Spectra. Int J Radiat Oncol. 2015;93(3):557–568. doi:10.1016/j.ijrobp.2015.07.2264

[32]. Grimes DR, Warren DR, Partridge M. An approximate analytical solution of the Bethe equation for charged particles in the radiotherapeutic energy range. Sci Rep. 2017;7(1):9781. doi:10.1038/s41598-017-10554-0 [PubMed: 28852130]

[33]. Qin N, Pinto M, Tian Z, et al. Initial development of goCMC: a GPU-oriented fast cross-platform Monte Carlo engine for carbon ion therapy. Phys Med Biol. 2017;62(9):3682–3699. doi:10.1088/1361-6560/aa5d43 [PubMed: 28140352]

[34]. Grevillot L, Boersma DJ, Fuchs H, et al. Technical Note: GATE-RTion: a GATE/Geant4 release for clinical applications in scanned ion beam therapy. Med Phys. 2020;47(8):3675–3681. doi:10.1002/mp.14242 [PubMed: 32422684]

[35]. Wang W, Huang Z, Sheng Y, et al. RBE-weighted dose conversions for carbon ionradiotherapy between microdosimetric kinetic model and local effect model for the targets and organs at risk in prostate carcinoma. Radiother Oncol J Eur Soc Ther Radiol Oncol. 2020;144:30–36. doi:10.1016/j.radonc.2019.10.005

[36]. Ma J, Wan Chan Tseung HS, Courneyea L, Beltran C, Herman MG, Remmes NB. Robust radiobiological optimization of ion beam therapy utilizing Monte Carlo and microdosimetric kinetic model. Phys Med Biol. 2020;65(15):155020. doi:10.1088/1361-6560/aba08b [PubMed: 32590359]

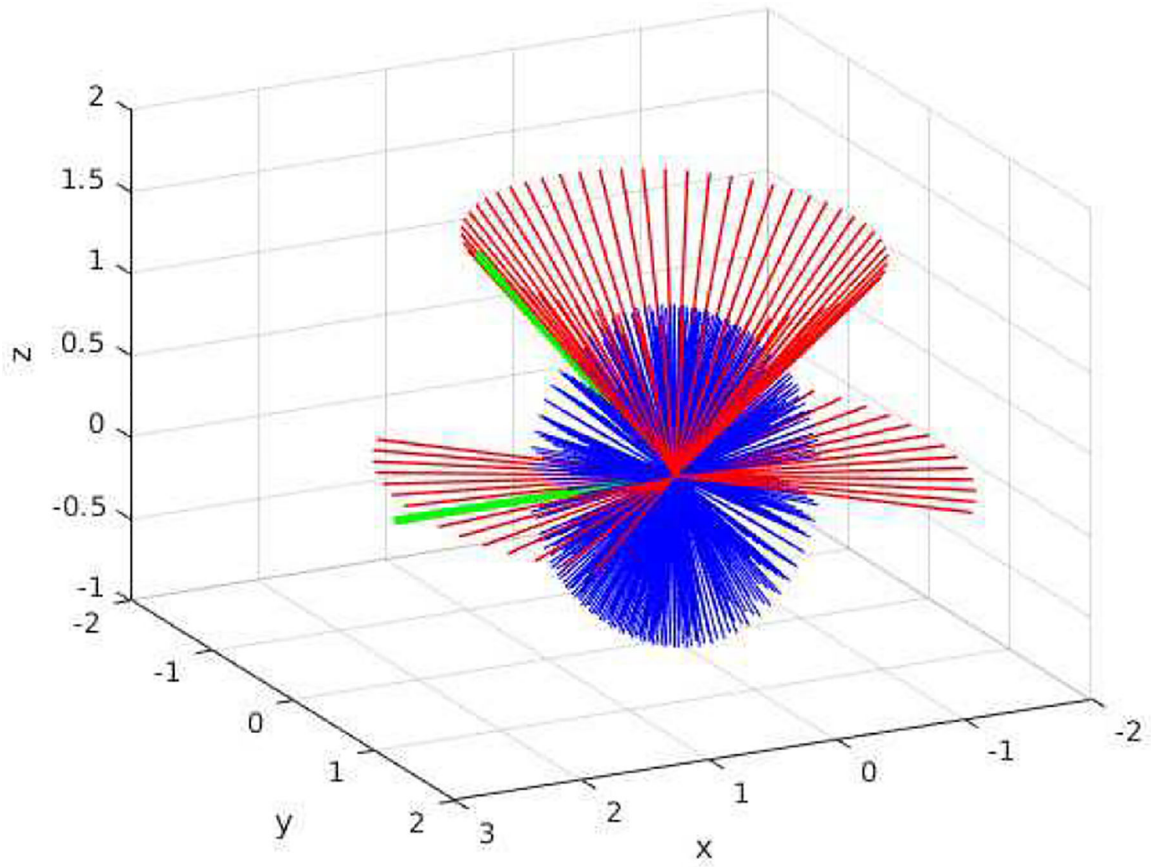

Fig. 1.

Candidate beams for GCR (blue), FBCR (red), and FB (green). The gantry-based plan includes 420 non-coplanar beams. FBCR includes 60 couch angles from the 45° and 30 from the 90° polar angles, and the FB plan includes one 45° and one 90° gantry angle, both with couch at 0°.

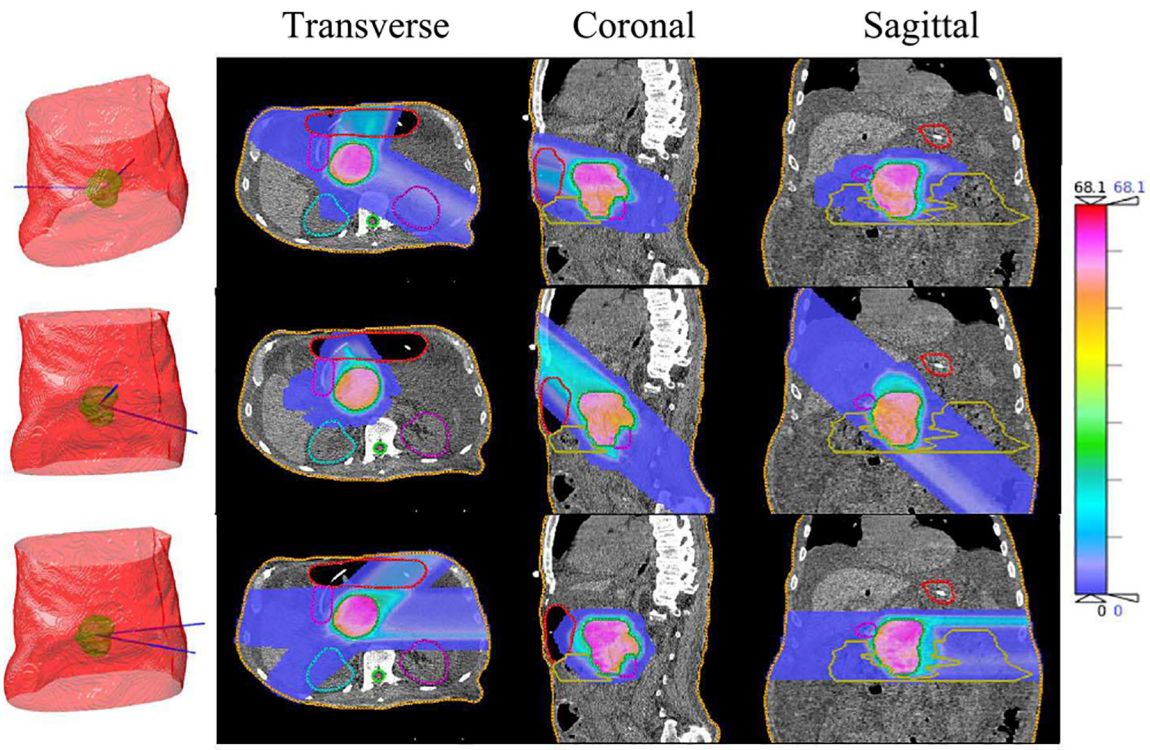

Fig. 2.

Beam orientation along with isodose comparison between GCR (top), FBCR (middle), and FB (bottom) plans for pancreas patient F.

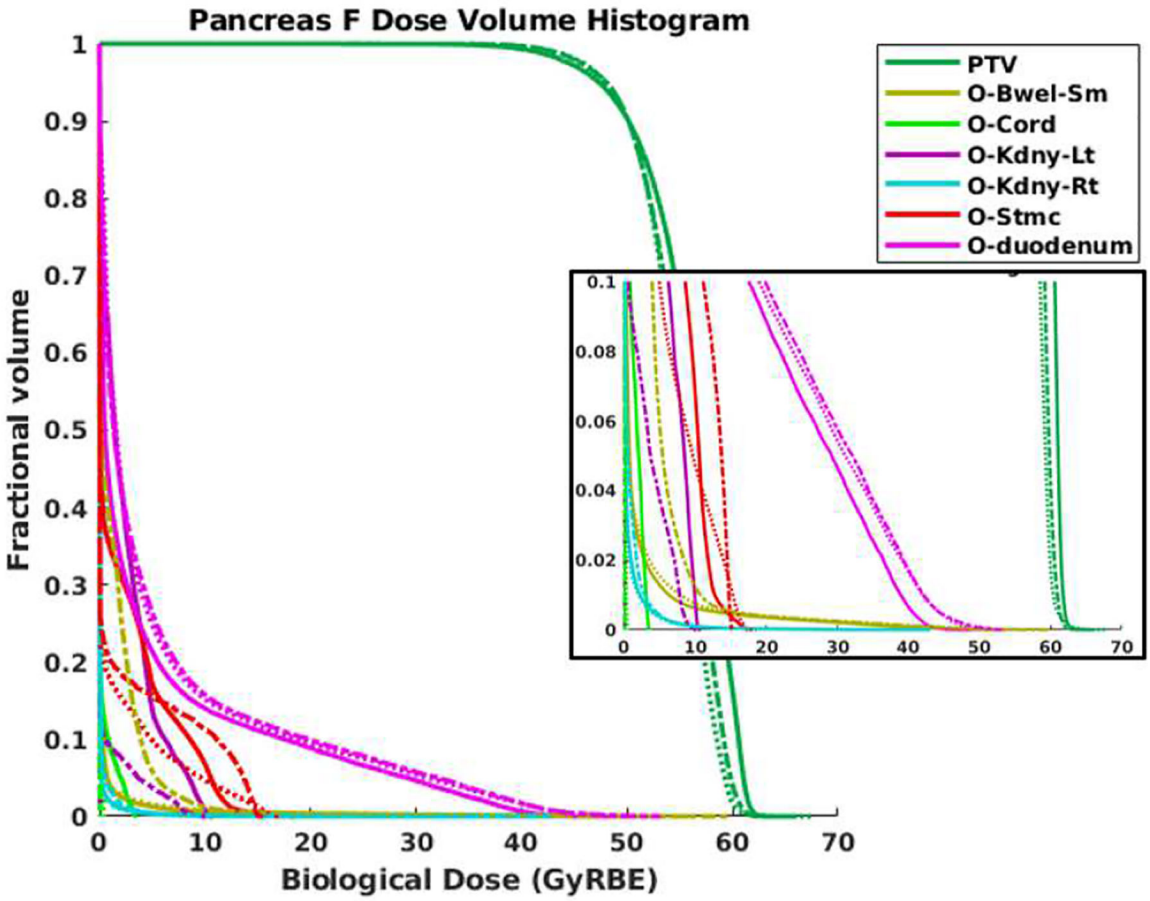

Fig. 3.

Dose-volume histogram for pancreas patient F. Solid lines represent the GCR, dotted lines represent FBCR, and dashed lines represent FB.

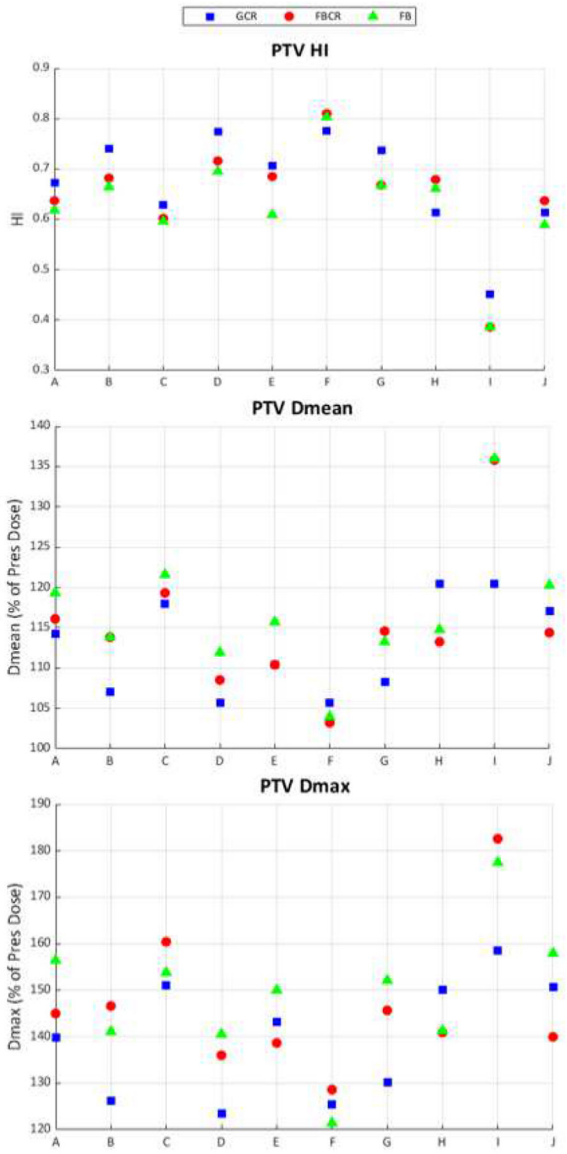

Fig. 4.

PTV statistics for all pancreatic cases. Dmax and Dmean are biological dose values represented as a percent of the prescribed dose to the PTV volume.

TABLE I

PTV volumes, and average number of spots per beam for each case.

Case	PTV Volume (cc)	Average Number of Spots per Beam
A	50.4	2044
B	128.2	4538
C	48.9	2037
D	41.0	1737
E	99.2	3475
F	268.0	7937
G	8.7	562
H	62.2	2393
I	91.3	3317
J	60.1	2309

TABLE II

Dose calculation and optimization times (minutes) with beam angles (degrees) selected for each plan. For GCR plans, both gantry and couch angles were determined by the BOO algorithm. For FBCR plans, couch angles were determined by BOO, and for FB plans, both beams were fixed.

	Dose Calculation Time, BOO Time (min)			Beams Selected (gantry, couch)		
	GCR	**FBCR**	**FB**	**GCR**	**FBCR**	**FB**
A	15.5	3.1	3.1	(210,39)	(45,246)	(45,0)
	2.9	2.0	1.2	(140,29)	(90,222)	(90,0)
B	55.1	12.1	12.1	(140,331)	(45,54)	(45,0)
	6.6	3.0	2.8	(35,33)	(45,174)	(90,0)
C	14.0	2.8	2.8	(205,46)	(45,276)	(45,0)
	2.3	2.5	1.1	(25,346)	(90,222)	(90,0)
D	14.5	2.9	2.9	(54,0)	(45,114)	(45,0)
	2.4	0.9	0.8	(322,340)	(45,354)	(90,0)
E	36.3	7.6	7.6	(25,314)	(45,78)	(45,0)
	5.2	3.9	2.1	(149,348)	(45,294)	(90,0)
F	117	19.0	19.0	(135,26)	(45,258)	(45,0)
	12.9	5.6	5.4	(220,331)	(90,42)	(90,0)
G	5.6	1.1	1.1	(153,332)	(45,126)	(45,0)
	0.5	0.3	0.4	(315,334)	(45,144)	(90,0)
H	29.9	6.3	6.3	(125,345)	(90,215)	(45,0)
	3.0	2.9	1.9	(198,270)	(90,330)	(90,0)
I	28.7	6.8	6.8	(330,39)	(45,198)	(45,0)
	4.9	2.8	2.1	(161,288)	(45,276)	(90,0)
J	17.3	4.0	4.0	(155,346)	(45,342)	(45,0)
	2.6	1.4	1.2	(347,333)	(90,138)	(90,0)

TABLE III

OAR dose results for the pancreatic cases.

	Structure	GCR	FBCR	FB
A	Bowel	**3.5**	7.1	13.7
	Duodenum	**1.0**	2.6	3.1
	Stomach	**0.2**	0.6	3.9
	Spinal Cord	5.8	0.2	**0.1**
B	Bowel	**0.1**	0.8	10.4
	Duodenum	**36.0**	40.0	37.4
	Stomach	**0.1**	**0.1**	**0.1**
	Spinal Cord	1.9	**0.1**	**0.1**
C	Bowel	**0.1**	**0.1**	**0.1**
	Duodenum	**40.8**	43.0	42.4
	Stomach	**0.3**	0.8	4.7
	Spinal Cord	9.6	**0.1**	**0.1**
D	Bowel	**0.1**	**0.1**	**0.1**
	Duodenum	5.1	**2.9**	4.9
	Stomach	0.2	**0.1**	0.3
	Spinal Cord	**0.1**	**0.1**	**0.1**
E	Bowel	**6.1**	9.3	13.7
	Duodenum	24.4	**24.0**	24.6
	Stomach	**25.0**	27.4	27.6
	Spinal Cord	14.5	**0.1**	**0.1**
F	Bowel	**31.7**	34.2	35.2
	Duodenum	**34.1**	36.5	37.2
	Stomach	15.1	16.2	**14.9**
	Spinal Cord	3.6	**0.1**	**0.1**
G	Bowel	0.4	**0.1**	4.6
	Duodenum	**7.6**	8.6	12.9
	Stomach	**0.7**	2.2	4.6
	Spinal Cord	2.1	**0.1**	**0.1**
H	Bowel	49.1	49.6	**47.8**
	Stomach	**0.3**	1.4	0.7
	Spinal Cord	5.5	**0.1**	**0.1**
I	Bowel	**25.5**	30.0	28.6
	Stomach	**6.8**	12.5	22.3
	Spinal Cord	11.7	0.3	**0.1**
J	Bowel	**28.5**	28.9	30.4
	Duodenum	**12.4**	**12.4**	13.3
	Stomach	**0.1**	**0.1**	**0.1**
	Spinal Cord	11.1	**0.1**	**0.1**

Maximum biological dose received by 2cc (D2cc) of bowel, duodenum, and stomach and maximum biological dose (Dmax) to spinal cord. All values are reported in GyRBE.